# Optimization of Controllable-Pitch Propeller Operations for Yangtze River Sailing Ships

N.B. When citing this work, cite the original published paper.

(article starts on next page)

*Article*

# Optimization of Controllable-Pitch Propeller Operations for Yangtze River Sailing Ships

Wuliu Tian [1,2], Xiao Lang [3,*], Chi Zhang [3], Songyin Yan [1,2,*], Bing Li [1,2] and Shuo Zang [4]

1   Transportation System and Safety Engineering Research Institute for Pinglu Canal, Beibu Gulf University, Qinzhou 535000, China; tianwuliu@foxmail.com (W.T.); 13306539486@163.com (B.L.)
2   College of Maritime, Beibu Gulf University, Qinzhou 535000, China
3   Department of Mechanics and Maritime Sciences, Chalmers University of Technology, 412 96 Gothenburg, Sweden; chizha@chalmers.se
4   Center of National Waterborne Transport Safety, Wuhan University of Technology, Wuhan 430062, China; shuo.zang@whut.edu.cn
*   Correspondence: xiao.lang@chalmers.se (X.L.); ysymsaysy@126.com (S.Y.)

**Abstract:** The Yangtze River's substantial variation in water depth and current speeds means that inland ships face diverse operational conditions within a single voyage. This paper discusses the adoption of controllable-pitch propellers, which adjust their pitch to adapt to varying navigational environments, thereby optimizing energy efficiency. We developed an optimization framework to determine the ideal pitch angle and rotation speed (RPM) under different sailing conditions. The energy performance model for inland ships was enhanced to account for the open-water efficiency of CPPs across various pitch angles and RPMs, considering the impacts of current and shallow water, among other factors. The optimization approach was refined by incorporating an improved genetic algorithm with an annealing algorithm to enhance the initial population, applying the K-means clustering algorithm for population segmentation, and using multi-parent crossover from diverse clusters. The efficacy of the optimization method for CPP operations was validated by analyzing three operational scenarios of a Yangtze sailing ship. Additionally, key components of the ship performance model were calibrated through experimental tests, demonstrating an anticipated fuel consumption reduction of approximately 5% compared to conventional fixed-pitch propellers.

**Keywords:** inland shipping; controllable-pitch propeller; fuel consumption; open-water efficiency; genetic algorithm; energy efficiency; ship–engine–propeller match

## 1. Introduction

Inland shipping on the Yangtze River is an important mode of water transportation in China, known for its low pollution, minimal land use, and large transport capacity. Due to stricter regulations, a growing public awareness of emissions from inland vessels, and the uncertainty of fuel prices, shipping companies operating in the Yangtze River are under considerable pressure to enhance their ships' energy efficiency and reduce energy consumption. The majority of ships on the Yangtze today use fixed-pitch propellers. However, the diverse hydrological conditions across different areas of the river and different seasons lead to generally inefficient propulsion for most of the time. In contrast, controllable-pitch propellers (CPPs) enable rotation of propeller blades through an integrated hub mechanism, allowing adjustment of the angle between the propeller and the hub. Compared to fixed-pitch propellers, changing the pitch angle of CPPs can help adjust sailing speed and maintain propeller performance based on navigation conditions. Using CPPs helps ships adapt better to changes in navigation environments and speeds, which can lower ship fuel consumption and improve energy efficiency. The essence of optimal CPP operations involves optimizing the alignment of the ship, engine, and propeller by adjusting the pitch angle and rotation speed.

The reliability of ship performance models is critical for such optimization methods. Matínez-López et al. [1] analyzed the environmental performance of ship optimization using the turbulent Reynolds average equation. Kim and Kinnas [2] introduced numerical techniques based on potential flow theory for adjusting the propeller pitch, which involved rotating the propeller blade. Jaurola et al. [3] reviewed ship system configurations and power management strategies to maximize power system benefits. For assisting ship operations, empirical formulas such as those by Holtrop and Mennen [4] have been widely used to estimate a ship's performance during navigation. These models were developed further by Lang and Mao [5,6]. Kristensen and Lützen [7] built new empirical models based on full-scale measurement data. With the advent of digitalization in shipping, substantial data on ship performance monitoring have been employed for modeling using machine learning techniques [8–10], with comparisons of different algorithms in Lang et al. [11]. Lang et al. [12] also combined empirical models with machine learning to increase the accuracy of performance modeling.

In the realm of ship operational optimization, low-fidelity empirical models have attracted attention due to their balance between computational speed and reasonable accuracy in predictions. Lu et al. [13] developed a low-fidelity optimization method based on Kwon's approach to minimize fuel consumption for an oil tanker. Tillig et al. [14] employed the semi-empirical ship model ShipCLEAN to optimize ship speed and minimize fuel consumption over given voyages, utilizing weather statistics from Monte Carlo simulations. Yang et al. [15] applied the low-fidelity DTU-SDU model, achieving a relatively low error rate in fuel consumption predictions per hour across various ship routes and optimizing the case-by-case ship operation. Another study by Li et al. [16] explored the application of ITTC ship models for container ships' operation optimization, aiming to refine cost optimization on specific routes. Fan et al. [17] utilized a generic model based on regression analysis that considered current speed to optimize cruise ship operations through dynamic programming. Tzortzis and Sakalis [18] used a semi-empirical model to optimize ship speed and minimize a container ship's fuel consumption. Various methodologies using low-fidelity models have been proposed for CPP optimization, including coupling propeller design tools with nonlinear optimizers [19], employing Particle Swarm Optimization algorithms to minimize fuel consumption [20], implementing sliding mode control strategies to enhance CPP system performance [21], and developing joint controllers with load protection for optimal matching control of engine speed and pitch [22]. To optimize ship engine and propeller design, Ren et al. [23] conducted detailed studies on optimizing pitch and ship–engine–propeller alignment, linking it to the Energy Efficiency Design Index (EEDI) and demonstrating how the EEDI varies with changes in navigation parameters. Tadros et al. [24] developed an optimization program for adjustable-pitch propellers to optimize parameters such as propeller diameter, pitch, and speed with fuel consumption as the target. Geertsma et al. [25] proposed a diesel engine propulsion model based on the principle of equal value priority. This model incorporates a baseline control strategy that utilizes a fixed combination curve, an acceleration limit, and pitch angle control, enabling reliable predictions of the propulsion system's behavior. Alessandri et al. [26] designed PID controllers for adjusting a vessel's heading and speed, optimizing parameters using a linearized model, and testing against external disturbances. Altosole et al. [27] presented the rapid prototyping and testing of a propulsion controller for an Italian aircraft carrier using real-time hardware-in-the-loop (RT HIL) to predict the propulsion plant's behavior under different working conditions. Coraddu et al. [28] estimated the optimal efficiency settings for a propulsion plant in real seaway conditions by integrating seakeeping and powering simulations. Figari et al. [29] proposed a "dynamic set point" control strategy for controllable-pitch propeller to reduce fuel consumption. Martelli et al. [30] developed a controllable-pitch propeller numerical model to describe ship propulsion dynamics through time-domain simulation. Michetti et al. [31] reported how a Navy multi-mission frigate equipped with controllable-pitch propellers reduces operational costs in daily operations while maintaining safety under various conditions.

Most research on optimizing fuel consumption for CPP ships has focused on maritime transport [32–34]. For inland shipping, it is crucial to consider factors such as the shallow-water effect and hull–propeller interaction, as reported by Kulczyk and Tabaczek [35]. A notable characteristic of inland waterways is that strong currents significantly influence navigation, presenting unique operational conditions for downstream and upstream navigation. Particularly for Yangtze shipping, the navigation conditions, such as water depth and current, change markedly across different sections and seasons. This paper establishes a ship fuel consumption–propeller pitch–diesel engine speed relationship model. An enhanced genetic algorithm optimization model was also developed to minimize fuel consumption by finding optimal pitch and speed settings for various navigation conditions. The structure of the remainder of this paper is as follows: Section 2 briefly describes performance modeling for CPP ship operations. Section 3 introduces the proposed genetic optimization method for CPP operations in Yangtze River navigation. Case-study ship and demonstration scenarios are introduced in Section 4. Section 5 presents the optimization results from the proposed method, compared across three predefined operational scenarios. Section 6 summarizes key conclusions.

## 2. Performance Modeling of CPP Inland Ships

To study a ship's fuel consumption, it is essential to correctly model the three subcomponents of its energy system: the ship hull, propeller, and engine. The efficiency analysis of a controllable-pitch propeller is more complicated than that of a fixed-pitch propeller due to their open-water efficiency changing under different pitch angles.

### 2.1. Ship Resistance in Inland Waterways

The total resistance $R$ of inland sailing ships can be divided into calm-water resistance $R_{CALM}$ and added resistance $\Delta R$:

$$R = R_{CALM} + \Delta R, \tag{1}$$

where $R_{CALM}$ refers to the resistance of the underwater part of the ship to water and is only affected by ship draft and sailing speed. The added resistance $\Delta R$ contains various components, such as wind and waves. The sailing environments of inland waterways are not as severe as those encountered in oceanic conditions; factors such as waves and wind are comparatively mild. Consequently, the effect of the added resistance is not considered in this study. The impact of shallow water on $R_{CALM}$ is substantial. This influence is accounted for through a correction factor in the following modeling process.

Various empirical formulas are available to model the calm-water resistance of inland vessels. In this study, the Holtrop and Mennen formulas [4], developed through full-scale trials and model experiments with a series of ship types, have been employed to estimate the calm-water resistance. The equation is defined as follows:

$$R_{CALM} = R_f(1 + k_1) + R_r, \tag{2}$$

where $R_f$ is the frictional resistance, estimated by the ITTC-1957 frictional correlation line [36], and the empirical formulas are used to calculate the form factor $1 + k_1$. The residual resistance $R_r$ includes the resistance of the appendages, immersed transom, etc.

It is important to note that shallow-water effects are crucial in influencing fuel consumption for inland shipping. Inland waterways, particularly natural river channels, experience periodic changes in current with the seasons, which are important to consider because the current speed affects the calculation between a ship's speed through water and speed over ground. As a ship navigates in shallow water, the water flow between the bottom of the ship and the riverbed narrows, constraining the movement of water molecules and increasing frictional resistance. The impact of shallow water on ship resis-

tance is primarily related to ship speed and the ratio of water depth to ship draft. This study estimates the shallow-water effect on total resistance as follows [37]:

$$R = K_h R_f + R_r, \text{ with } K_h = 1 + 0.57 \left(\frac{h}{d}\right)^{-1.79}, \tag{3}$$

where the total resistance $R$ includes the shallow-water effect, $h$ is the channel water depth, and $d$ is the ship draft. The validity range of this correction formula is $\frac{h}{d} > 2$.

### 2.2. Thrust and Torque of CPPs

During navigation, ship propellers convert the torque from the engine into thrust via rotation. To maintain a constant speed $V$, the propeller propulsion compensates by delivering the necessary torque to overcome the ship's resistance $R$, enabling the propeller to generate an equivalent thrust $T = R$. The propeller thrust $T$ and torque $Q$ are given as follows:

$$T = K_T \rho n^2 D^4, Q = K_Q \rho n^2 D^5, \tag{4}$$

where $K_T$ and $K_Q$ are the thrust and torque coefficients, respectively; $D$ is the propeller diameter; and $n$ denotes the propeller RPM. For fixed-pitch propellers, thrust and torque can be estimated using regression calculations from efficiency charts [2]. However, the calculation for a CPP involves more complex relationships between the thrust and torque coefficients and the advance ratio and pitch angle.

In the absence of sufficient data to fit the CPP's thrust and torque coefficients at various pitches, this study utilizes the OpenProp code [38] to analyze the open-water performance of the CPP. Open-water efficiency at different pitches is interpolated based on the original pitch's experimental curve. The CPP blade is modeled as a lifting line, with induced velocity calculated by a vortex mesh, ensuring that the trailing vortex aligns with local flow velocity. Each blade section's properties are analyzed discretely along its radius, integrating 2D section loads across the blade width to compute the blade load. $V_a$ and $V_t$ represent the axial and tangential inflow velocities, while $u_a^*$ and $u_t^*$ denote the induced axial and tangential velocities. $r$ refers to the radius, as depicted in Figure 1.
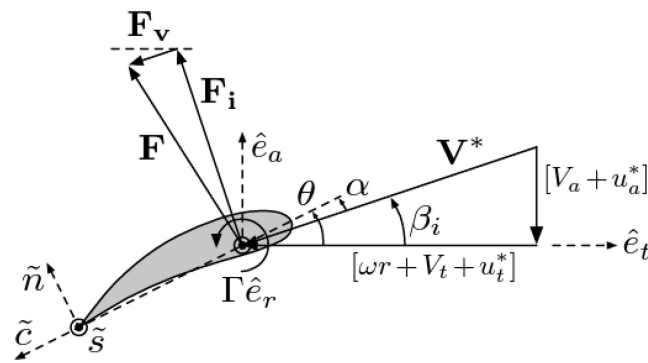


**Figure 1.** Controllable-pitch propeller force diagram [38].

The corresponding pitch angle is calculated by $\beta = arctan(V_a + u_a^*/wr + V_t + u_t^*)$. Using the OpenProp code, the geometry of the CPP allows for an estimation of thrust and torque by integrating across the propeller's geometry. Subsequently, the open-water efficiency of the propeller at a particular pitch can be estimated as follows:

$$\eta_0 = \frac{T \cdot V_a}{Q \cdot 2\pi \cdot n} = \frac{K_T}{K_Q} \cdot \frac{J_S}{2\pi}, \ J_S = \frac{V_a}{nD}, \tag{5}$$

where $J_S$ is the advance ratio, a crucial parameter in describing the propeller's operational characteristics. It is defined as the ratio of the propeller's forward travel to its diameter during one complete rotation. The wake fraction $\omega$, the thrust deduction factor $t$, and

the relative rotative efficiency $\eta_R$ are calculated by the well-known empirical formula for twin-screw ships as proposed by Holtrop and Mennen [4].

## 2.3. Fuel Consumption Modeling

Building upon the established empirical models for ship resistance and CPP propulsion efficiency, the simplified process of ship–engine–propeller matching is illustrated in Figure 2. The Specific Fuel Oil Consumption (SFOC, expressed in g/kWh) of the ship engine is crucial for estimating the total fuel consumption, and the fuel consumption per hour $G$ in g/h is calculated as follows [39]:

$$G = P_B \cdot SFOC = \frac{P_E}{\eta_0 \eta_H \eta_R \eta_s} \cdot SFOC. \tag{6}$$

where $\eta_H$ represents the hull efficiency, $\eta_o$ is the open-water efficiency, and $\eta_s$ is the shaft efficiency. The effective power $P_E$ can be expressed as follows:
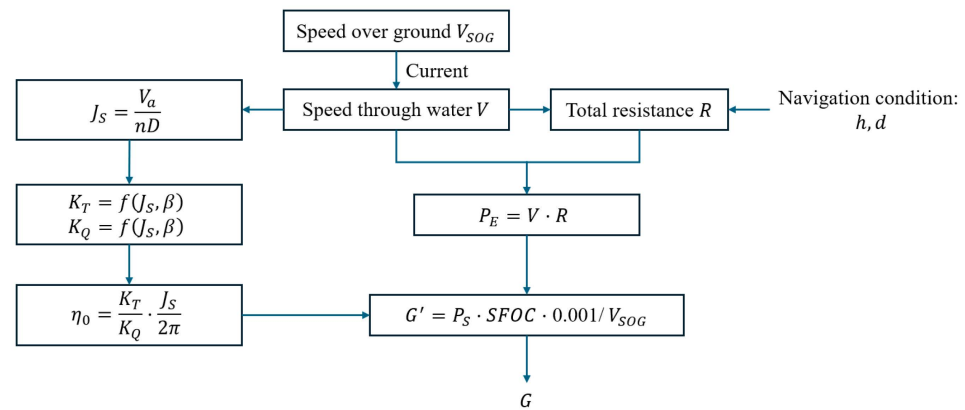
$$P_E = R \cdot V. \tag{7}$$



**Figure 2.** The simplified CPP ship fuel consumption modeling process in this study.

Based on these calculations, a model can be established to explore the interdependencies among the propeller pitch, the engine, and the ship's fuel consumption. First, the modified inland navigation resistance formula determines resistance at specific draft $d$, current speed $u$, and water depth $h$. Subsequent analysis of the performance of the CPP facilitates the generation of open-water curve diagrams for varying pitches. These diagrams depict the functional relationship among the thrust coefficient $K_T$, torque coefficient $K_Q$, open-water efficiency $\eta_0$, advance coefficient $J_S$, and pitch angle $\beta$. The ship's fuel consumption per nautical mile is then given as follows [39]:

$$G' = 0.001 \cdot P_B \cdot SFOC / V_{SOG}, \tag{8}$$

where $G'$ is the fuel consumption rate in kg/mile and $V_{SOG}$ is the ship speed over ground. This model establishes the relationship between ship fuel consumption and propeller pitch. This study applies the SFOC curve at different engine loads provided by the ship owner. However, certain pitch and RPM combinations may lead to issues such as thrust resistance mismatch, negative thrust, and inadequate propeller structural strength Thus, in the optimization process, the pitch–fuel consumption model cannot be applied directly. Instead, a further optimization process and specific constraint conditions must be established to achieve the lowest possible fuel consumption while ensuring stable operation of the CPP.

### 3. Voyage Optimization Method Based on Improved Genetic Optimization

*3.1. Description of the Voyage Optimization Problem*

First, a ship voyage is discretized into *m* legs, and it is assumed that the ship sails with the same propeller pitch angle *β* and RPM n for each leg where the water depth and current remain unchanged. The control variables $X$ to be optimized for an individual voyage are denoted by the following:

$$X = [x_1, x_2, \ldots, x_i, \ldots, x_n], \ x_i = [\beta_i, n_i], \tag{9}$$

where $\beta_i$ and $n_i$ represent the propeller pitch angle and RPM at the *i*th leg of the voyage. In this study, the optimization task is to find optimal $X$ that can minimize the fuel consumption for a specific sailing time as follows:

$$\hat{X} = \underset{X \in R}{\arg \min} \frac{A_1 G(x_1) + A_2 G(x_2) + \ldots + A_n G(x_n)}{\sum_{i=1}^{m} A_i}, \tag{10}$$

where $A_i$ is the optimization weight of a given leg.

The optimization process is illustrated in Figure 3. The operation optimization begins with Step 1, which involves setting up all the parameters, such as the number of legs, initial settings for each leg, and sailing time. The optimization algorithm used in this study, a genetic algorithm (Step 2), takes all initial conditions to evaluate the ship's performance in Step 3 and to assess the cost function in Step 4. In Step 3, various components outlined in Section 2 are analyzed to find the optimal match among ship speed, RPM, and propeller pitch. The cost function for the control parameters is then evaluated in Step 4. The optimal value is updated when the new input yields a lower objective function value. By repeating this process, the optimal solution can be obtained.
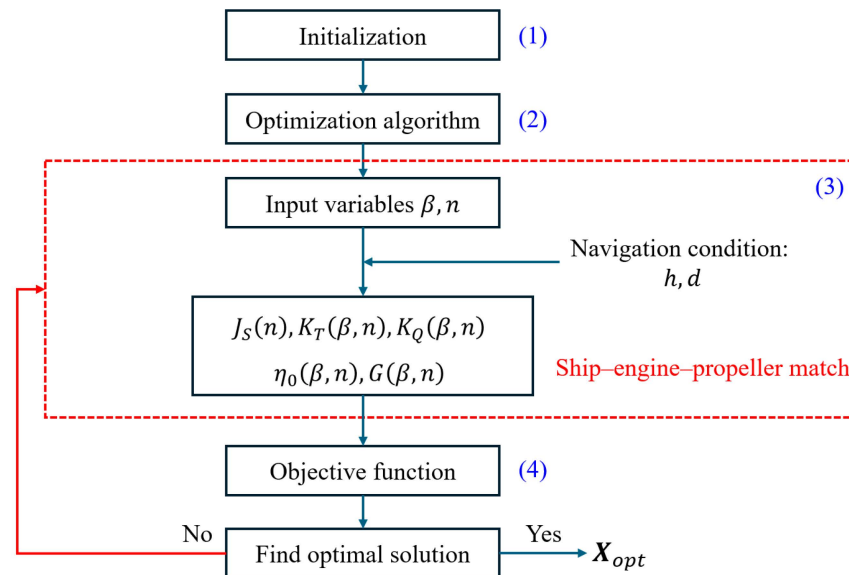


**Figure 3.** The proposed CPP operation optimization method in this study.

*3.2. Genetic Algorithm for Optimization*

The genetic algorithm represents a refined suite of search optimization methods inspired by the evolutionary principles of natural species. This algorithm mimics the processes of natural selection, reproduction, and genetic variation, enabling the generation of superior solutions [40], as illustrated in Figure 4. Initially, the genetic algorithm establishes a population where individuals are encoded. It then proceeds by calculating fitness values for these individuals using a predefined fitness function. The fittest individuals are selected based on these values, and crossover and mutation operations are performed on them.

Individuals with suboptimal fitness are eliminated, which facilitates the generation of a new population. This cyclical process of selection, crossover, and mutation continues until the stipulated criteria for population iteration are met, leading to the identification of an optimal solution.
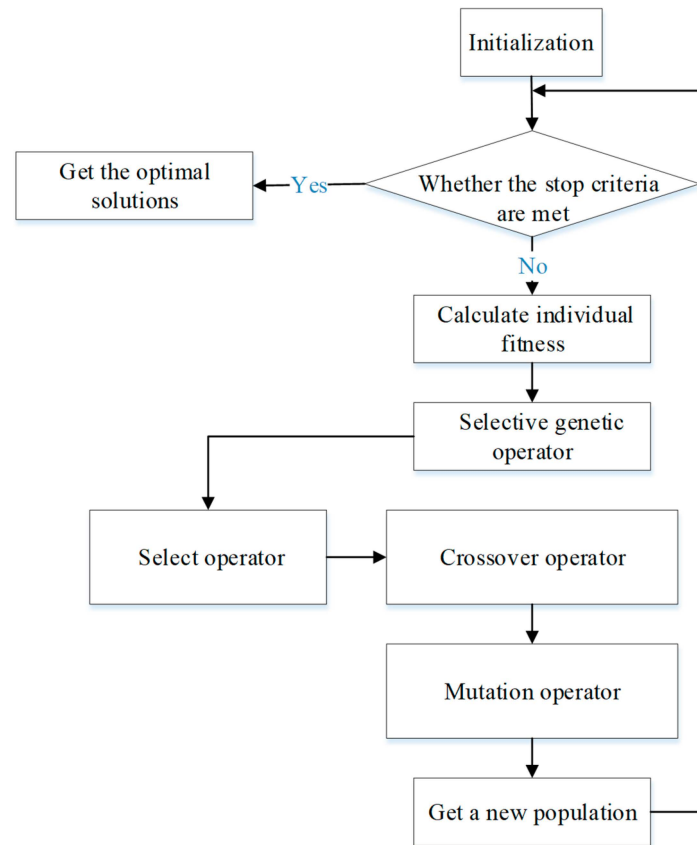


**Figure 4.** Conventional genetic algorithm optimization process.

However, traditional genetic algorithms encounter several challenges. They are heavily dependent on the quality of the initial population, which can significantly influence their efficiency and outcomes. Additionally, these algorithms often progress slowly in optimization tasks and risk converging to suboptimal solutions due to their stochastic nature and limited exploration capabilities.

*3.3. Proposed Improvement to the Genetic Algorithm for Voyage Optimizations*

3.3.1. Algorithm Initialization

To enhance the performance of the genetic algorithm, particularly by addressing its inherent limitations, this study proposes integrating the simulated annealing algorithm to generate the algorithm's initial solutions. This integration is depicted in Figure 5 and involves several key steps:

1.  Initial setup: Set a sufficiently high initial temperature $T$ to ensure acceptance of a considerable number of transition states. Randomly generate the initial solution $S$, and set the number of iterations at each temperature to $L$.
2.  Iteration process: In each iteration, generate a new solution $S_i$. Calculate the energy change $\Delta E = S_{i+1} - S_i$. If the energy decreases, the state is accepted. Conversely, if the energy increases, the state is accepted with a probability computed as $e^{-\frac{\Delta E}{T_i}}$, where $T_i$ is the current temperature.
3.  Cooling schedule: Gradually decrease the temperature according to the formula $T(i+1) = \alpha T(i)$, where $\alpha$ is the cooling rate.

4.  Termination check: Determine whether the temperature has reached the termination condition. If so, conclude the annealing process, and add the optimal generated solutions to the initial population of the genetic algorithm.
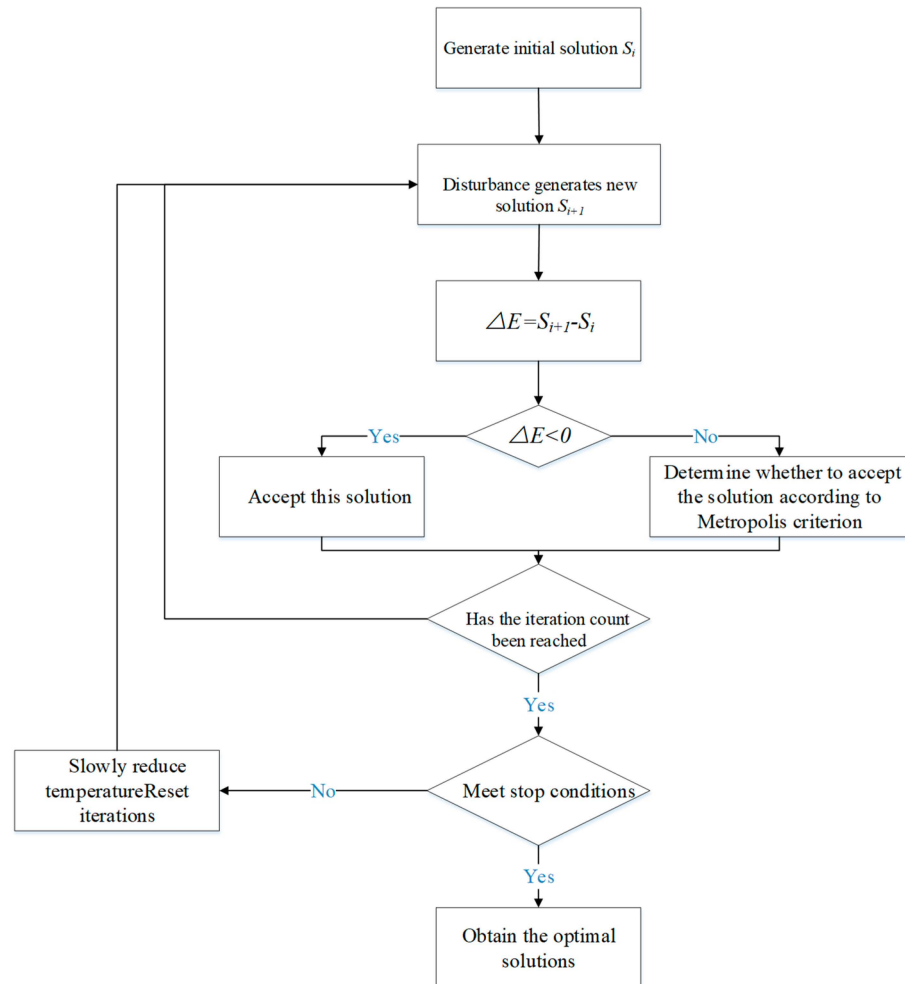


**Figure 5.** The further improved method for generating the initial genetic algorithm population by adding the annealing algorithm.

3.3.2. Elite Retention Strategy Based on Exponential Function

In the selection phase of the genetic algorithm, conventional methods such as tournament or roulette selection present a risk of inadvertently removing the most capable individuals from the population. This study introduces an innovative strategy to address these challenges: a variable-proportion elite retention approach based on an exponential function. The replication ratio is dynamically adjusted, increasing at a rate determined by an exponential function and eventually reaching stability, as depicted in Equation (11):

$$K = 0.1 + ln(q)t, \tag{11}$$

where $t$ is the replication coefficient, $q$ represents the number of evolutions, and $K$ is the proportion of the number of optimal elite individuals in the parent population that are directly copied to the new offspring population relative to the total population. This strategy effectively ensures the preservation of superior elite parental individuals over their less advantageous counterparts.

### 3.3.3. Multi-Parent Crossover Strategy Based on the K-Means Algorithm

In the default crossover strategy, deficiencies may arise when randomly selected individuals possess very similar genetics. To address this issue, the integration of K-means clustering and multi-parent crossover techniques is proposed. This process involves segmenting the population into clusters based on low genetic similarity and then selecting individuals from diverse clusters for crossover. This approach not only enhances the quality of the crossover but also increases the overall genetic diversity within the population.

The chromosome length is assumed to be *lchrom*. Each chromosome is represented as a vector in Euclidean space according to its distinct genes, denoted as $x = (x_1, x_2, \ldots x_{lchrom})$, and the Euclidean distance between it and another chromosome $y = (y_1, y_2, \ldots y_{lchrom})$ is defined as follows:

$$d_{xy} = \sqrt{\sum_{k=1}^{n}(x_k - y_k)^2}. \tag{12}$$

Based on the population size, an appropriate number of clusters is determined, and individuals are randomly selected from the chromosome dataset as initial cluster centers. Once the individuals are categorized, the distance from each individual to its cluster center is calculated and compared. Using the minimum distance criterion, individuals are classified into the cluster where the nearest center point is located. The cluster center is then updated according to the following formula:

$$Z_i^{(w+1)} = \frac{1}{C_i^w} \sum_{x_j \in C_i} x_j. \tag{13}$$

where $Z_i^{(w+1)}$ is the cluster center point determined after the $w$th update and $C_i^w$ is the cluster set after the update. Categories are refreshed based on the updated cluster centers, and if no change occurs in the cluster centers after two consecutive updates, the algorithm is deemed to have converged, completing the clustering process. Subsequently, the multi-parent genetic operator is employed, selecting three individuals at random from three distinct clusters identified using the K-means algorithm, as illustrated in Figure 6.
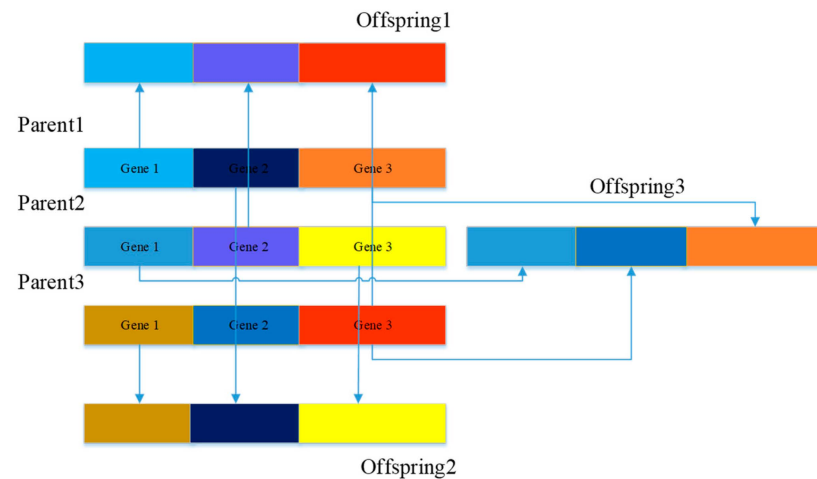


**Figure 6.** Schematic diagram of the further developed crossover strategy.

### 3.3.4. Combination Mutation Strategy

In the mutation phase, the distinct advantages of various mutation operators are leveraged to optimize the search process. This study employs a composite mutation strategy, where a random integer within the range of [1,3] is generated for each generation. The integer dictates the specific mutation operator to be applied:

- Gaussian mutation for 1, which focuses on local refinement,
- Uniform mutation for 2, offering a balanced approach to the search strategy,
- BGA mutation for 3, which is designed to enhance global exploration.

This dynamic strategy adapts to the ongoing search process, facilitating effective navigation of the solution space. By cycling through these mutation strategies, the algorithm effectively balances exploration and exploitation, thereby enhancing the efficiency and effectiveness of identifying optimal solutions.

## 4. Case-Study Ship and Demonstration Scenarios

### 4.1. Case-Study Ship and Division of Sailing Sections

This study used a 64TEU inland ship as the case-study ship (Taizhou Sanfu Heavy Industry Group Co., Ltd., Taizhou, China). The ship's resistance, open-water propulsion efficiency, and engine load curve were modeled and validated through experimental tests. Details of the modeling and validation processes are outlined in the subsequent subsections. Table 1 displays the case-study ship's main characteristics and propeller parameters. The ship was equipped with two outward-rotating propellers. Detailed specifications of these propellers are provided in the table below.

**Table 1.** Main parameters of the 64TEU inland case-study ship and the installed propellers.

| Ship Parameter | Value | Propeller Parameter | Value |
|---|---|---|---|
| Ship length | 67.50 m | Diameter | 1.693 m |
| Waterline length | 66.35 m | Number of blades | 5 |
| Ship breadth | 12.67 m | Original pitch ratio | 0.75 |
| Molded depth | 3.30 m | Disk ratio | 0.5 |
| Propulsion power | $2 \times 240$ KW | Hub diameter | 0.29 m |
| Spacing of fins | 0.55 m | Hub length | 0.32 m |
| Gross tonnage (DWT) | 990 tons | Back angle | 10° |

Experimental tests were also conducted to understand the resistance at varying speeds for the case-study ship in this study. A comparison between the resistance estimated by Equations (1) and (2) and those obtained from experimental tests revealed some discrepancies. Consequently, the Holtrop and Mennen empirical formulas were calibrated for the case-study ship's resistance. Calibration factors were selected through a sensitivity analysis focused on the parameters most affecting resistance, specifically the correction coefficients related to the ship speed and Froude number. Polynomial regression was then applied to calibrate the empirical formulas as follows:

$$R_{CALM} = 9^{(0.162(V-4))} F_r{}^{-0.5} (R_f (1 + k_1) + R_r). \tag{14}$$

The resistance calculated using the calibrated formula, as depicted in Equation (14), is compared with experimental data in Figure 7 for the case-study ship, which has a draft of 2.4 m, representing 70% of its full load capacity. It is evident that, following calibration, the empirical-formula-derived resistance closely matched the experimental results. Consequently, this calibrated formula was employed in subsequent modeling and simulations. The SFOC at different engine loads applied in this study is shown in Figure 8.

Based on the pitch–fuel consumption model outlined in Section 2, the propeller pitch and RPM can be optimized to minimize the fuel consumption of the case-study ship for the desired ETA. In this study, three distinct operational scenarios were applied for simulation:

- Scenario 1: The ship sails at a constant speed (7 knots) and draft (2.4 m).
- Scenario 2: The ship operates at variable speeds (4, 7, and 11 knots) while maintaining a constant draft (2.4 m), specifically during downstream navigation (segments 7–14).
- Scenario 3: The ship maintains a constant speed (7 knots) with variable drafts (1.2 and 2.4 m) and is engaged in a round trip including downstream voyages (segments 7–14).
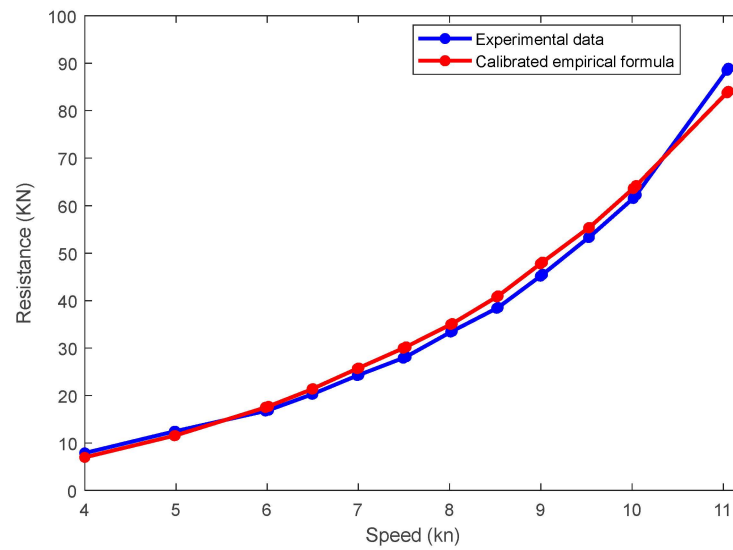
**Figure 7.** Comparison of the ship resistance for the case-study ship, with a draft of 2.4 m; the blue line is experimental data, and the red line is the results from the calibrated formula.
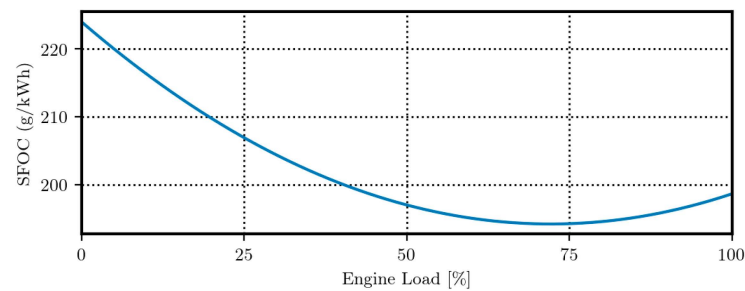


**Figure 8.** The SFOC at different engine loads as percentages of the maximum continuous rating (MCR) for the case-study ship.

The optimization aimed to optimize fuel consumption for the equipped CPP case-study ship operating along the Yangtze River trunk line. The division of the Yangtze River trunk line is based on the relevant data published by the Yangtze River Channel Bureau, "2023 Yangtze River Trunk Line Channel Maintenance Scale Standard". The depth, curvature, and other data are shown in Table 2.

**Table 2.** Division of the Yangtze River sections.

| Segments | Voyage | Water Depth (m) | Current Velocity (m/s) | Bending Radius (m) | Mileage (km) |
|---|---|---|---|---|---|
| 1 | Yibin Hejiangmen–Chongqing Yangjiaotan | 2.9 | 0.766 | 560 | 207 |
| 2 | Chongqing Yangjiaotan–Fuling Lidu Yangtze River Bridge | 3.5 | 0.472 | 800 | 60 |
| 3 | Fuling Lidu Yangtze River Bridge–Ziguimiao River | 5.5 | 0.467 | 1000 | 293 |
| 4 | Ziguimiao River–Songzi Kuabaoshan | 4.5 | 0.945 | 750 | 40 |
| 5 | Songzi Kuabaoshan–Jingzhou Port | 3.8 | 1.144 | 1000 | 42 |
| 6 | Jingzhou Port–Yueyang Chenglingji | 3.8 | 1.164 | 1000 | 135 |
| 7 | Yueyang Chenglingji–Wuhan Yangtze River Bridge | 4.5 | 1.222 | 1000 | 124 |
| 8 | Wuhan Yangtze River Bridge–Anqing Jiyangji | 6.0 | 1.16 | 1050 | 206 |
| 9 | Anqing Jiyangji–Wuhu Gao'anwei | 6.0 | 1.183 | 1050 | 106 |
| 10 | Wuhu Gao'anwei–Wuhu Yangtze River Bridge | 7.5 | 1.131 | 1050 | 20 |
| 11 | Wuhu Yangtze River Bridge–Nanjing Yanziji | 9.0 | 1.154 | 1050 | 55 |
| 12 | Nanjing Yanziji–Nanjing Xinshengwei | 10.5 | 1.036 | 1050 | 2 |
| 13 | Nanjing Xinshengwei–Jiangyin Yangtze River Bridge | 12.5 | 0.98 | 1500 | 98 |
| 14 | Jiangyin Yangtze River Bridge–Yangtze River Estuary | 12.5 | 0.8 | 1500 | 83 |

### 4.2. CPP Propulsion Efficiency Modeling for the Case Study Ship

A CPP with predefined geometry has hydrodynamic characteristics that are influenced by the pitch and advance ratio. For the case-study ship, the propeller geometry

was available and was utilized by the OpenProp software (version 3.3.4) to estimate the propulsion efficiency across various pitch angles and advance ratios. Initially, to validate the accuracy of the OpenProp model, the calculated open-water efficiency at the service pitch angle of the case study ship was compared with experimental test results (provided by the ship owner), as illustrated in Figure 9. The calculated thrust coefficient and torque coefficient were slightly lower than the experimental outcomes. Additionally, when the advance ratio was low, the open-water efficiency exceeded that measured; however, it fell below the experimental results as the advance ratio $J_S$ increased. The overall error margin was less than 6%. This discrepancy arose due to the theoretical simplifications incorporated in the OpenProp calculations. While improving the precision of open-water efficiency calculations is beyond the scope of this paper, this level of computational error is unlikely to significantly impact the subsequent optimization results. In the future, we plan to employ higher-fidelity CFD methods to minimize these errors.
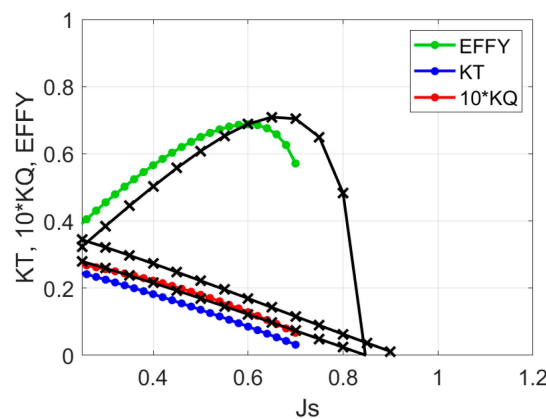


**Figure 9.** Comparison of measured and calculated open-water efficiency: the black curve represents the experimental measurements, while the curves in various colors correspond to calculations from OpenProp software.

Subsequently, the OpenProp software was employed to analyze the open-water performance of the propeller at various pitch angles (we assumed that all angles were truly feasible in terms of the mechanical limits of the CPP's actuating mechanism). The thrust and torque curves for nine different pitch angles were assessed, including the service pitch, service pitch $\pm$ 3 degrees, service pitch $\pm$ 5 degrees, service pitch $\pm$ 7 degrees, and service pitch $\pm$ 10 degrees. Following the estimation of open-water efficiency for these predefined pitch angles, the performance of the propeller at other pitch angles was predicted using linear interpolation analysis. Figures 10 and 11 display some of the estimated and interpolated open-water curves for the controllable-pitch propeller.
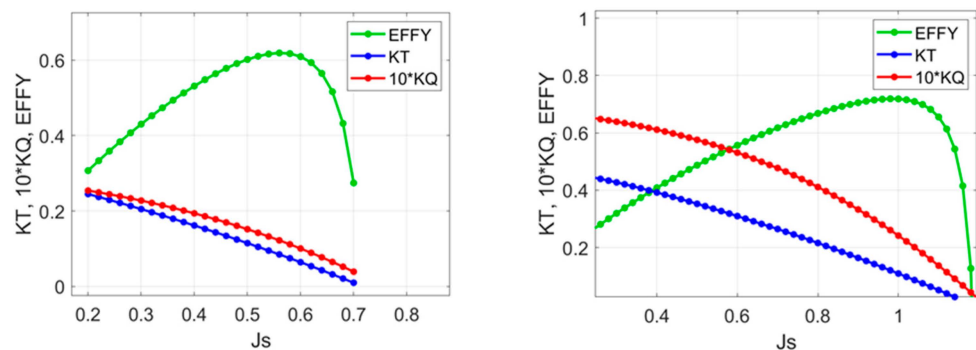


**Figure 10.** Open-water efficiency for pitch angles of service pitch angle $+3°$ (**left**) and $+7°$ (**right**).
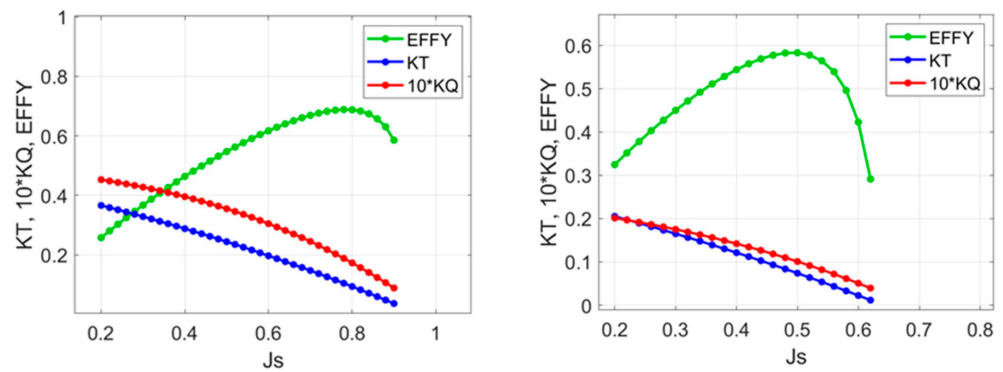
**Figure 11.** Open-water efficiency for pitch angles of service pitch angle $-5°$ (**left**) and $-3°$ (**right**).

Figure 12 shows the open-water efficiency of the case-study CPP at different pitch angles. The propeller's open-water performance at higher speeds improves as the pitch angle decreases. However, the propeller's peak efficiency point is slightly below that observed at larger pitch angles. Therefore, it is possible for CPP-equipped vessels to adjust the propeller pitch angles and rotation speeds according to specific navigational conditions, enabling the propeller to operate at its highest efficiency from a global optimization standpoint.
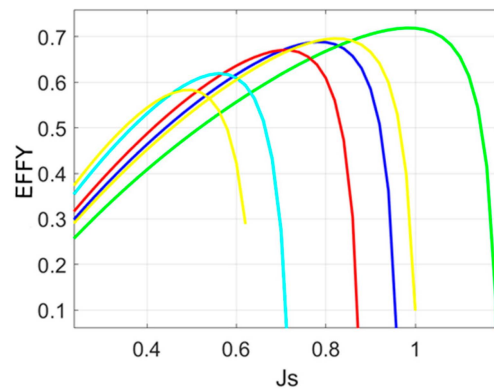


**Figure 12.** Open-water efficiency at different pitch angles for the case-study CPP; service pitch angles of $-3°$, $+3°$, $+4°$, $+5°$, $+6°$, and $+7°$ are presented from left to right.

### 4.3. Parameter Setting for the Improved Genetic Algorithm

As discussed Section 3.3, the improved genetic algorithm requires parameter settings at each step. To enhance the transparency of this study, the detailed optimization process and the parameter settings utilized in the improved genetic algorithm are outlined as follows:

1.  Range of input values: The upper and lower limits for the pitch angle were determined by OpenProp to be the original pitch angle $\pm 10$ degrees. This restriction was imposed because propeller efficiencies outside this range could cause the advance ratio to exceed the operational range of the diesel engine. The speed range was set according to the rated speed of the diesel engine, with the RPM variation range set between 500 and 1500, based on the characteristics of the case-study ship.
2.  Algorithm initialization: The initial population was generated using the simulated annealing algorithm, with an initial temperature set to 100 to allow acceptance of more transition states. The number of iterations, $L$, was set to 100, with an annealing rate of 0.9 to ensure rapid convergence. The termination temperature was set at 0, and the initial population size was 505.
3.  Selection: The selection process utilized the elite retention strategy as discussed in Section 3.3, with a replication coefficient of 0.03.
4.  Crossover: The crossover process employed a multi-parent crossover operator based on the K-means algorithm, with the number of clusters set to 50. Three individu-

als from different clusters were selected for random multi-parent crossover, with a crossover probability of 0.7.

5. Mutation: The mutation phase used a single-point mutation method with a mutation probability of 0.3. If offspring chromosomes generated during the crossover or mutation processes failed to meet constraints, the mutation or crossover was repeated until acceptable chromosomes were produced.

6. Termination condition: The stopping criterion for the algorithm was set such that the optimization process terminated either when the number of iterations reached 500 or if there was no decrease in the best fitness value across 10 subsequent iterations.

## 5. Results and Discussion

### 5.1. Optimization Results of Scenario 1

Based on the optimization model previously established, the optimization process for the case study in scenario 1 is depicted in Figure 13. The optimization process of segment 3 is shown in Figure 13 as an example. The fitness value progressively converged by the 545th generation. Figure 14 illustrates the optimized pitch angle and RPM across the 14 sections.
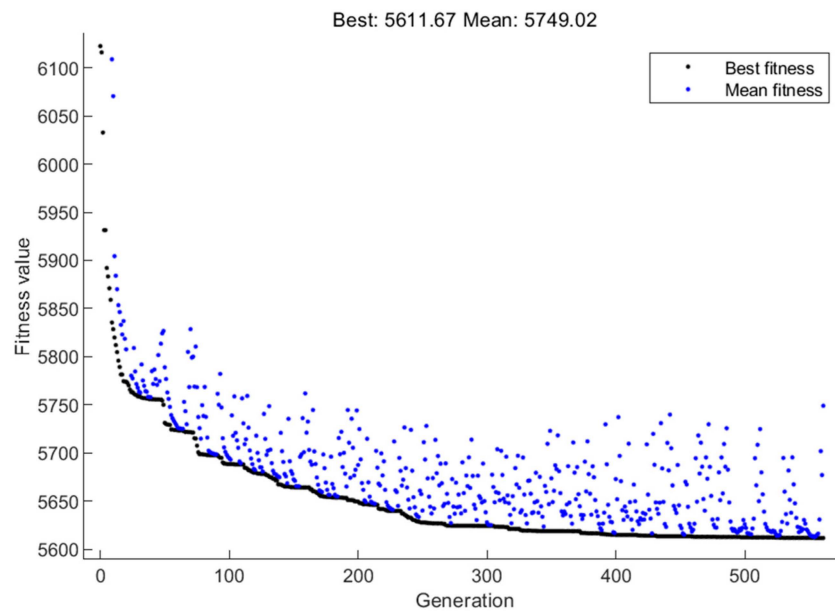


**Figure 13.** Optimization iteration for segment 3 of scenario 1; the blue dots are the mean fitness, and the black dots indicate the best fitness.
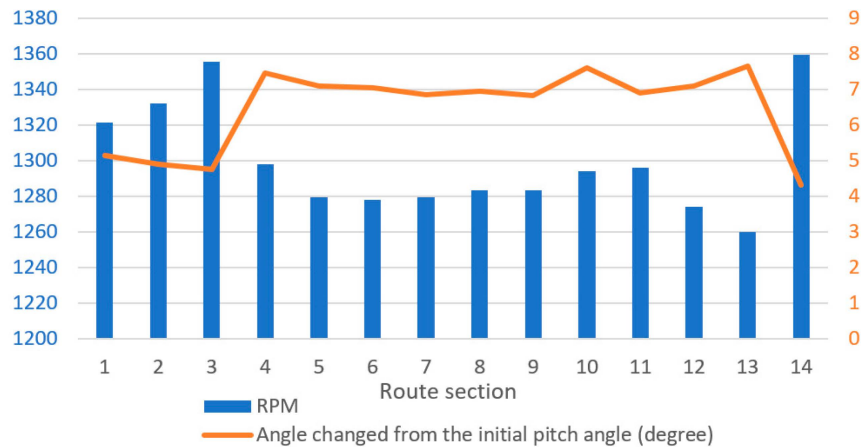


**Figure 14.** Optimal pitch angle and RPM of scenario 1.

Table 3 presents the specific values of the optimal pitch angle, RPM, and other parameters for each section. From these data, it is evident that the optimal pitch angles for segments 1 (Yibin Hejiangmen-Chongqing Yangjiaotan), 2 (Chongqing Yangjiaotan-Fuling Lidu Yangtze River Bridge), and 3 (Fuling Lidu Yangtze River Bridge-Ziguimiao River) show substantial variations. This variation is attributable to the fluctuating upstream water depths and relatively low water levels, which intensify the shallow-water effect during navigation. Notably, the section from Yibin Hejiangmen to the Ziguimiao River (route sections 1, 2, and 3) consistently exhibits the shallowest depths, necessitating additional pitch angle adjustments to optimize propeller efficiency against changing resistance.

**Table 3.** Optimization results of different segments.

| Voyage Segments | Optimal Pitch Angle (Degrees) | Optimum RPM | Thrust (kN) | Open-Water Efficiency |
|---|---|---|---|---|
| 1 | Original pitch angle + 5.13 | 1321.49 | 61.37 | 0.56 |
| 2 | Original pitch angle + 4.89 | 1332.04 | 61.32 | 0.55 |
| 3 | Original pitch angle + 4.75 | 1355.51 | 60.19 | 0.53 |
| 4 | Original pitch angle + 7.47 | 1297.98 | 56.71 | 0.61 |
| 5 | Original pitch angle + 7.09 | 1279.25 | 57.19 | 0.59 |
| 6 | Original pitch angle + 7.04 | 1278.16 | 57.26 | 0.59 |
| 7 | Original pitch angle + 6.85 | 1279.23 | 57.29 | 0.58 |
| .8 | Original pitch angle + 6.95 | 1283.17 | 56.63 | 0.58 |
| 9 | Original pitch angle + 6.84 | 1283.53 | 57.52 | 0.57 |
| 10 | Original pitch angle + 7.62 | 1294.16 | 57.91 | 0.63 |
| 11 | Original pitch angle + 6.89 | 1295.98 | 57.61 | 0.58 |
| 12 | Original pitch angle + 7.08 | 1273.98 | 57.32 | 0.55 |
| 13 | Original pitch angle + 7.65 | 1259.79 | 57.15 | 0.61 |
| 14 | Original pitch angle + 4.30 | 1359.43 | 59.17 | 0.56 |

Furthermore, the optimization outcomes reveal that larger optimal pitch angles typically require a corresponding decrease in diesel engine speed. This relationship arises because the peak of open-water efficiency shifts towards a higher advance ratio with changes in pitch. Given that the advance ratio is influenced solely by the RPM during constant speed navigation, an increase in the advance ratio is achieved by slightly reducing the RPM to accommodate the increase in pitch. However, variations in pitch angle also impact the relative rotational efficiency, leading to a less pronounced correlation between pitch angle and diesel engine speed in the optimization results.

The adjustment of the pitch angle maintains the propeller operation at a higher efficiency level throughout the navigation, thus mitigating adverse effects from the navigational environment. According to Table 3, the open-water efficiencies exceed 50%, with higher efficiency observed when the ship navigates through the midstream and downstream sections of the Yangtze River. This improvement is attributable to these sections being better suited to the ship's voyage, characterized by deeper water and milder currents. Additionally, the propeller achieves a higher maximum efficiency at larger pitch angles, and its maximum efficiency point shifts towards a higher advance ratio as the pitch angle increases.

Table 4 presents a comparison of the fuel consumption for the target ship before and after optimization. Under identical sailing conditions, load, and draft parameters, the ship's fuel consumption per voyage has decreased by approximately 4.78%.

**Table 4.** Comparison of fuel consumption between optimal pitch and fixed pitch.

| Pitch Allocation | Fuel Consumption of Single Voyage (kg) |
|---|---|
| Fixed at the original pitch | 5893.27 |
| Optimal pitch setting | 5611.67 |

### 5.2. Optimization Results of Scenario 2

In scenario 2, the case-study ship is set to navigate at three distinct speeds: high speed (11 knots), medium speed (7 knots), and low speed (4 knots), with equal navigation time allocated for each speed. The fuel consumption rate is employed as the objective function. As depicted in Figure 15, the fitness value progressively converged by the 65th generation at a speed of 4 kn. Figure 16 illustrates the optimized pitch angle and RPM across the three different speed settings.
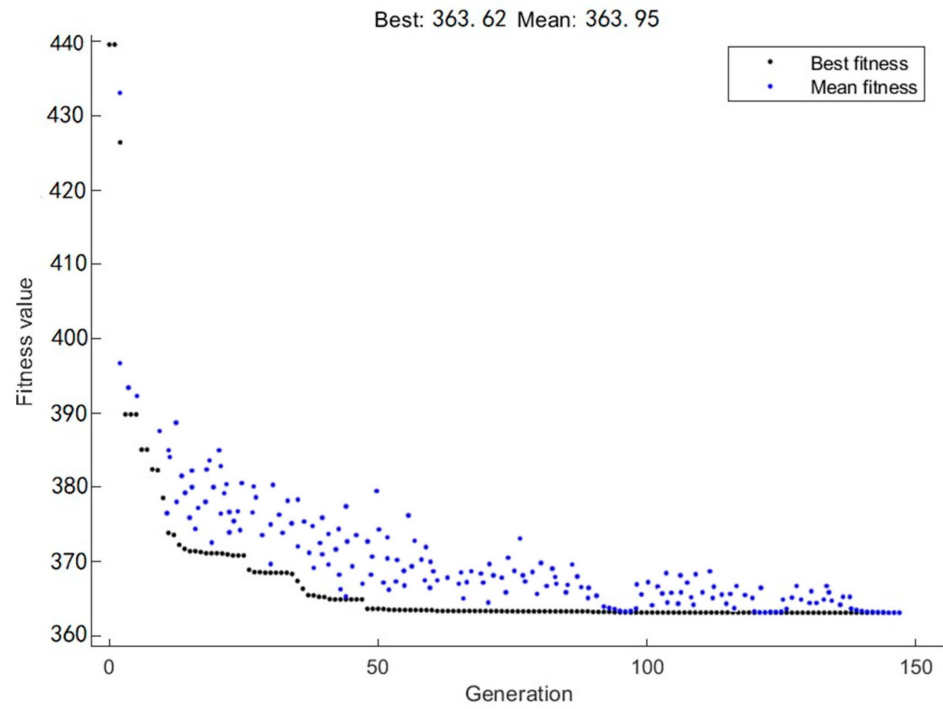


**Figure 15.** Optimization iteration at a speed of 4 kn in scenario 2; the blue dots are the mean fitness, and the black dots indicate the best fitness.
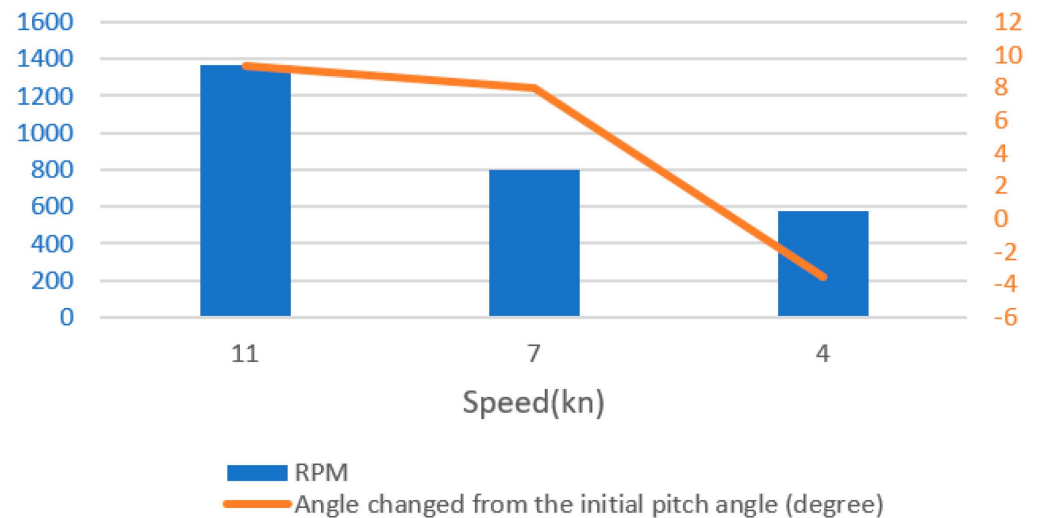


**Figure 16.** Optimal pitch angle and RPM for scenario 2.

As indicated in Table 5, the fuel consumption rate escalates sharply with increasing sailing speed, yet the propeller operates more efficiently than when sailing at low speeds. To further investigate the effect of sailing speed on the optimization outcomes, the ratio of the three speeds was varied. The results of these adjustments are displayed in Table 6.

**Table 5.** Optimization results of different speed settings.

| Speed (kn) | Pitch Angle (Degrees) | RPM | Thrust (KN) | Open-Water Efficiency | Fuel Consumption Rate (kg/nm) |
|---|---|---|---|---|---|
| 11 | Original pitch angle + 9.37 | 1369.76 | 105.31 | 0.59 | 263.60 |
| 7 | Original pitch angle + 7.96 | 798.64 | 37.65 | 0.56 | 75.35 |
| 4 | Original pitch angle − 3.51 | 578.31 | 19.57 | 0.46 | 23.67 |

**Table 6.** Optimization results of speed settings with different time ratios in scenario 2.

| | Speed (kn) | Proportion | Pitch Angle (Degrees) | Open-Water Efficiency | Thrust (KN) | Fuel Consumption (kg/nm) |
|---|---|---|---|---|---|---|
| Speed allocation 1 | 4 | 1/3 | Original pitch angle − 3.51 | 0.50 | 19.57 | 23.67 |
| | 7 | 1/3 | Original pitch angle + 7.96 | 0.56 | 37.65 | 75.35 |
| | 11 | 1/3 | Original pitch angle + 9.37 | 0.59 | 105.31 | 263.60 |
| Speed allocation 2 | 4 | 1/10 | Original pitch angle − 2.03 | 0.47 | 19.02 | 25.26 |
| | 7 | 1/2 | Original pitch angle + 5.35 | 0.56 | 37.91 | 76.23 |
| | 11 | 2/5 | Original pitch angle + 9.19 | 0.57 | 106.25 | 261.35 |
| Speed allocation 3 | 4 | 1/10 | Original pitch angle + 1.03 | 0.43 | 17.36 | 23.76 |
| | 7 | 4/5 | Original pitch angle + 6.23 | 0.57 | 39.51 | 79.71 |
| | 11 | 1/10 | Original pitch angle + 9.59 | 0.60 | 103.17 | 260.19 |

As evidenced by Table 6, the propeller achieves higher open-water efficiency at the lower speed in speed allocation 1 than in the other two allocations. In speed allocation 3, where the vessel predominantly sails at medium speed, the improved genetic algorithm tended to overlook the periods of high and low speed to some extent during optimization in an effort to minimize fuel consumption. This is reflected in the thrust data shown in Table 6; at a speed of 4 knots, the propeller generates a thrust of 23.76 KN, whereas the ship encounters a resistance of 25.03 KN, with the thrust amounting to only 95% of the resistance.

### 5.3. Optimization Results of Scenario 3

Scenario 3 is dedicated to analyzing the effects of changing current directions and variations in load on the optimization of CPP in the downstream waters of the Yangtze River. The goal is to minimize fuel consumption throughout the round-trip voyage. In this simulation, the ship travels downstream fully loaded (draft 2.4 m), whereas the return trip is made in ballast (draft 1.3 m). The optimal pitch angle and RPM for each leg of the journey are depicted in Figure 17. The outcomes of the optimization are presented in Table 7.
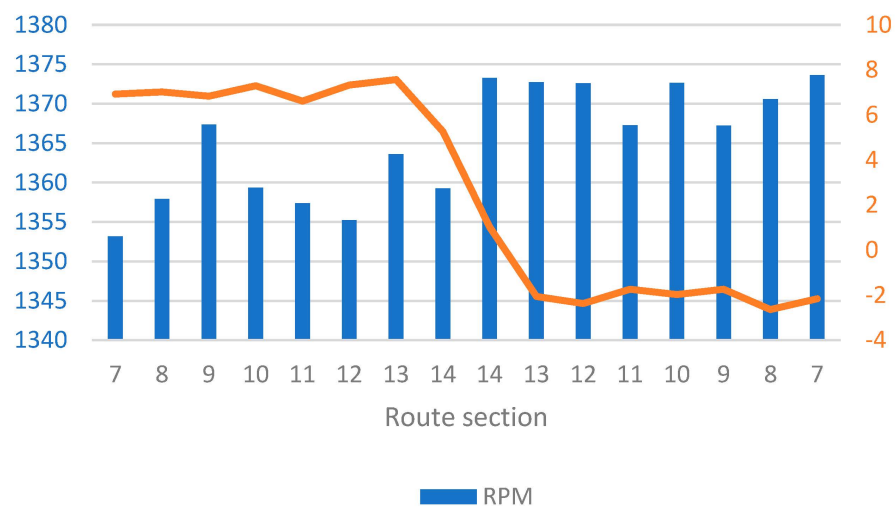


**Figure 17.** Optimization results of scenario 3.

**Table 7.** Optimization results of scenario 3.

| Direction | Voyage Segments | Pitch Angle (Degrees) | RPM | Open-Water Efficiency | Thrust (KN) |
|---|---|---|---|---|---|
| Forward | 7 | Original pitch angle + 6.92 | 1353.16 | 0.56 | 57.26 |
| | 8 | Original pitch angle + 7.02 | 1357.93 | 0.59 | 57.75 |
| | 9 | Original pitch angle + 6.83 | 1367.35 | 0.58 | 57.91 |
| | 10 | Original pitch angle + 7.29 | 1359.36 | 0.62 | 57.19 |
| | 11 | Original pitch angle + 6.61 | 1357.39 | 0.59 | 59.67 |
| | 12 | Original pitch angle + 7.32 | 1355.23 | 0.54 | 59.16 |
| | 13 | Original pitch angle + 7.57 | 1363.59 | 0.55 | 27.15 |
| | 14 | Original pitch angle + 5.26 | 1359.26 | 0.59 | 57.63 |
| Back | 14 | Original pitch angle + 1.02 | 1373.27 | 0.52 | 50.51 |
| | 13 | Original pitch angle − 2.06 | 1372.75 | 0.55 | 50.67 |
| | 12 | Original pitch angle − 2.37 | 1372.59 | 0.57 | 49.53 |
| | 11 | Original pitch angle − 1.73 | 1367.26 | 0.54 | 50.76 |
| | 10 | Original pitch angle − 1.97 | 1372.63 | 0.56 | 50.61 |
| | 9 | Original pitch angle − 1.73 | 1367.23 | 0.59 | 50.59 |
| | 8 | Original pitch angle − 2.63 | 1370.57 | 0.54 | 51.53 |
| | 7 | Original pitch angle − 2.16 | 1373.61 | 0.56 | 49.63 |

From Table 7, it is evident that the optimal pitch angle and RPM ranges for the two voyages differ significantly. This variation is primarily due to the change in water current direction, which alters the ship's speed and consequently affects the balance among the ship, engine, and propeller. Additionally, changes in the ship's draft significantly modify navigational resistance due to the shallower water effect. The results indicate that the open-water efficiency of the propeller is consistently maintained at a high level after optimization with the improved genetic algorithm. Table 8 displays the fuel consumption for the entire voyage before and after optimization, showing a reduction of 5.35% in total fuel consumption compared to sailing with a fixed-pitch propeller.

**Table 8.** Comparison of fuel consumption between controllable pitch and fixed pitch.

| Pitch Allocation | Fuel Consumption of Single Voyage (kg) |
|---|---|
| Fixed at the original pitch | 4698.74 |
| Optimal pitch setting | 4964.34 |

*5.4. Limitations of the Models Utilized*

The proposed framework indeed possesses inherent limitations. First, the modeling of ship resistance employs semi-empirical methods, which necessarily involve physical assumptions and simplifications based on regression analysis using datasets from diverse ship types. Consequently, predictions for a specific ship type at varying speeds inherently encompass a certain degree of uncertainty. This uncertainty arises from the regression process that averages data across different ship types, thereby leading to discrepancies when predictions are applied to individual ships. These discrepancies explain minor deviations such as those observed in Figure 7. Furthermore, the OpenProp software, an open-source computational tool, integrates theoretical simplifications into its calculations. Despite these simplifications, the software remains an appropriate tool for academic purposes, especially useful for computing the performance curve of a particular propeller design. The physical simplifications embedded within the software contribute to the prediction discrepancies noted in Figure 8. However, the primary objective of this study is not to design the propeller with high precision, but rather to optimize the operation of the CPP. The framework effectively captures the physical trends of the propeller across various settings for optimization purposes. In the subsequent phase, higher-fidelity CFD methods will be employed to model and calculate the propeller's performance and the ship's resistance, with the aim of mitigating the uncertainties observed in the current study.

## 6. Conclusions

This study introduces a framework for modeling the performance of ships equipped with controllable-pitch propellers operating in inland waterways, and an optimization method to identify optimal pitch angles and RPM for various sailing conditions to enhance energy efficiency. The performance model incorporates an experimentally calibrated empirical formula for resistance calculation, which is further adjusted to account for shallow-water effects. OpenProp software was utilized to calculate the open-water efficiency for different pitch angles and RPM settings. The optimization process was enhanced by integrating a simulated annealing algorithm to improve the quality of the initial population, employing a K-means clustering algorithm to segment the population, and selecting individuals from different classes for multi-parent crossover. Three operational scenarios of a Yangtze sailing ship were analyzed to validate the proposed optimization method for CPP operations. Key components of the ship performance model were also validated through experimental tests, demonstrating that the proposed method can achieve an approximate 5% reduction in fuel consumption compared to conventional fixed-pitch propellers. However, this study currently has limitations in simulation accuracy. Our model has the potential for application across various inland waterways. However, our access was limited to data from vessels operating on the Yangtze River, which guided our decision to conduct the case study within this specific context. Future work will involve using actual ship data to validate the effectiveness of the proposed framework. Additionally, we will employ higher-fidelity CFD methods to reduce the uncertainty of open-water efficiency and to better understand the hull-propeller interaction across various speeds and drafts.

**Institutional Review Board Statement:** Not applicable.

**Informed Consent Statement:** Not applicable.

**Data Availability Statement:** The dataset is not publicly available due to confidentiality agreements with the data provider.

**Conflicts of Interest:** The authors declare no conflicts of interest. The funders had no role in the design of the study; in the collection, analyses, or interpretation of data; in the writing of the manuscript; or in the decision to publish the results.

## References

1. Matínez-López, A.; Díaz Ojeda, H.R.; Míguez González, M.; Marrero, Á. Environmental Inefficiencies of Short Sea Shipping Vessels by Optimization Processes Based on Resistance Prediction Methods. *J. Mar. Sci. Eng.* **2022**, *10*, 1457. [CrossRef]
2. Kim, S.; Kinnas, S.A. A panel method for the prediction of unsteady performance of ducted propellers in ship behind condition. *Ocean Eng.* **2022**, *246*, 110582. [CrossRef]
3. Jaurola, M.; Hedin, A.; Tikkanen, S.; Huhtala, K. Optimising Design and Power Management in Energy-Efficient Marine Vessel Power Systems: A Literature Review. *J. Mar. Eng. Technol.* **2019**, *18*, 92–101. [CrossRef]
4. Holtrop, J.; Mennen, G. An Approximate Power Prediction Method. *Int. Shipbuild. Prog.* **1982**, *29*, 166–170. [CrossRef]
5. Lang, X.; Mao, W. A Semi-Empirical Model for Ship Speed Loss Prediction at Head Sea and Its Validation by Full-Scale Measurements. *Ocean Eng.* **2020**, *209*, 107494. [CrossRef]
6. Lang, X.; Mao, W. A Practical Speed Loss Prediction Model at Arbitrary Wave Heading for Ship Voyage Optimization. *J. Mar. Sci. Appl.* **2021**, *20*, 410–425. [CrossRef]
7. Kristensen, H.O.; Lützen, M. Prediction of resistance and propulsion power of ships. *Clean Shipp. Curr.* **2012**, *1*, 1–52.
8. Gupta, P.; Rasheed, A.; Steen, S. Ship Performance Monitoring Using Machine-Learning. *Ocean Eng.* **2022**, *254*, 111094. [CrossRef]

9. Mittendorf, M.; Nielsen, U.D.; Bingham, H.B. Capturing the Effect of Biofouling on Ships by Incremental Machine Learning. *Appl. Ocean Res.* **2023**, *138*, 103619. [CrossRef]

10. Kim, Y.-R.; Steen, S. Application of Machine Learning Algorithms for Predicting Added Resistance in Arbitrary Wave Headings of a Ship. In Proceedings of the OMAE, Hamburg, Germany, 5–10 June 2022.

11. Lang, X.; Wu, D.; Mao, W. Comparison of Supervised Machine Learning Methods to Predict Ship Propulsion Power at Sea. *Ocean Eng.* **2022**, *245*, 110387. [CrossRef]

12. Lang, X.; Wu, D.; Mao, W. Physics-Informed Machine Learning Models for Ship Speed Prediction. *Expert Syst. Appl.* **2024**, *238*, 121877. [CrossRef]

13. Lu, R.; Turan, O.; Boulougouris, E.; Banks, C.; Incecik, A. A Semi-Empirical Ship Operational Performance Prediction Model for Voyage Optimization towards Energy Efficient Shipping. *Ocean Eng.* **2015**, *110*, 18–28. [CrossRef]

14. Tillig, F.; Ringsberg, J.W.; Psaraftis, H.N.; Zis, T. Reduced Environmental Impact of Marine Transport through Speed Reduction and Wind Assisted Propulsion. *Transp. Res. Part D Transp. Environ.* **2020**, *83*, 102380. [CrossRef]

15. Yang, L.; Chen, G.; Zhao, J.; Rytter, N.G.M. Ship Speed Optimization Considering Ocean Currents to Enhance Environmental Sustainability in Maritime Shipping. *Sustainability* **2020**, *12*, 3649. [CrossRef]

16. Li, X.; Sun, B.; Guo, C.; Du, W.; Li, Y. Speed Optimization of a Container Ship on a given Route Considering Voluntary Speed Loss and Emissions. *Appl. Ocean Res.* **2020**, *94*, 101995. [CrossRef]

17. Fan, A.; Wang, Z.; Yang, L.; Wang, J.; Vladimir, N. Multi-Stage Decision-Making Method for Ship Speed Optimisation Considering Inland Navigational Environment. *Proc. Inst. Mech. Eng. Part M J. Eng. Marit. Environ.* **2021**, *235*, 372–382. [CrossRef]

18. Tzortzis, G.; Sakalis, G. A Dynamic Ship Speed Optimization Method with Time Horizon Segmentation. *Ocean Eng.* **2021**, *226*, 108840. [CrossRef]

19. Tadros, M.; Ventura, M.; Guedes Soares, C. Optimization Procedures for a Twin Controllable Pitch Propeller of a ROPAX Ship at Minimum Fuel Consumption. *J. Mar. Eng. Technol.* **2023**, *22*, 167–175. [CrossRef]

20. Bacciaglia, A.; Ceruti, A.; Liverani, A. Controllable Pitch Propeller Optimization through Meta-Heuristic Algorithm. *Eng. Comput.* **2021**, *37*, 2257–2271. [CrossRef]

21. Wang, Y.; Wang, Q.; Fu, H. Online High Performance Genetic Algorithm Based Sliding Mode Control for Controllable Pitch Propeller. *Processes* **2020**, *8*, 953. [CrossRef]

22. Ji, M.; Zhao, P.; Liang, L.; Liu, R. Design and Optimization of Control System for Controllable Pitch Propeller with Load Protection. In Proceedings of the 2018 IEEE International Conference on Mechatronics and Automation (ICMA), Changchun, China, 5–8 August 2018; pp. 1037–1042.

23. Ren, H.; Ding, Y.; Sui, C. Influence of EEDI (Energy Efficiency Design Index) on Ship–Engine–Propeller Matching. *J. Mar. Sci. Eng.* **2019**, *7*, 425. [CrossRef]

24. Tadros, M.; Ventura, M.; Guedes Soares, C. Optimum Design of a Container Ship's Propeller from Wageningen B-Series at the Minimum BSFC. In *Sustainable Development and Innovations in Marine Technologies*; CRC Press: Boca Raton, FL, USA, 2019; pp. 269–276.

25. Geertsma, R.D.; Negenborn, R.R.; Visser, K.; Loonstijn, M.A.; Hopman, J.J. Pitch Control for Ships with Diesel Mechanical and Hybrid Propulsion: Modelling, Validation and Performance Quantification. *Appl. Energy* **2017**, *206*, 1609–1631. [CrossRef]

26. Alessandri, A.; Donnarumma, S.; Vignolo, S.; Figari, M.; Martelli, M.; Chiti, R.; Sebastiani, L. System control design of autopilot and speed pilot for a patrol vessel by using LMIs. In *Towards Green Marine Technology and Transport*; CRC Press: Boca Raton, FL, USA, 2015; pp. 577–583.

27. Altosole, M.; Benvenuto, G.; Figari, M.; Campora, U.; Bagnasco, A.; D'Arco, S.; Giuliano, M.; Giuffra, V.; Spadoni, A.; Zanichelli, A. Real-time simulation of the propulsion plant dynamic behaviour of the aircraft carrier "Cavour". In Proceedings of the Institute of Marine Engineering, Science and Technology-INEC, Hamburg, Germany, 1–3 April 2009; pp. 123–130.

28. Coraddu, A.; Figari, M.; Savio, S.; Villa, D.; Orlandi, A. Integration of seakeeping and powering computational techniques with meteo-marine forecasting data for in-service ship energy assessment. *Dev. Marit. Transp. Exploit. Sea Resour.* **2014**, *1*, 93–101.

29. Figari, M.; Soares, C.G. Fuel consumption and exhaust emissions reduction by dynamic propeller pitch control. In Proceedings of the 2nd International Conference on Marine Structures-Analysis and Design of Marine Structures, Lisbon, Portugal, 16–18 March 2009; pp. 567–574.

30. Martelli, M.; Figari, M.; Altosole, M.; Vignolo, S. Controllable pitch propeller actuating mechanism, modelling and simulation. *Proc. Inst. Mech. Eng. Part M J. Eng. Marit. Environ.* **2014**, *228*, 29–43. [CrossRef]

31. Michetti, S.; Ratto, M.; Spadoni, A.; Figari, M.; Altosole, M.; Marcilli, G. Ship control system wide integration and the use of dynamic simulation techniques in the Fremm project. In Proceedings of the Electrical Systems for Aircraft, Railway and Ship Propulsion, Bologna, Italy, 19–21 October 2010; pp. 1–6.

32. Rudzki, K.; Tarelko, W. A Decision-Making System Supporting Selection of Commanded Outputs for a Ship's Propulsion System with a Controllable Pitch Propeller. *Ocean Eng.* **2016**, *126*, 254–264. [CrossRef]

33. Tarelko, W.; Rudzki, K. Applying Artificial Neural Networks for Modelling Ship Speed and Fuel Consumption. *Neural Comput. Appl.* **2020**, *32*, 17379–17395. [CrossRef]

34. Geertsma, R.D.; Visser, K.; Negenborn, R.R. Adaptive Pitch Control for Ships with Diesel Mechanical and Hybrid Propulsion. *Appl. Energy* **2018**, *228*, 2490–2509. [CrossRef]

35. Kulczyk, J.; Tabaczek, T. Coefficients of Propeller-Hull Interaction in Propulsion System of Inland Waterway Vessels with Stern Tunnels. *TransNav Int. J. Mar. Navig. Saf. Sea Transp.* **2014**, *8*, 377–384. [CrossRef]
36. ITTC. *Resistance Uncertainty Analysis Example for Resistance Test. Recommended Procedures*; 7.5-02-02-02; ITTC: Zürich, Switzerland, 2002.
37. Raven, H. A New Correction Procedure for Shallow-Water Effects in Ship Speed Trials. In Proceedings of the 13th International Symposium on Practical Design of Ships (PRADS 2016), Copenhagen, Denmark, 4 September 2016.
38. Epps, B.P.; Stanway, M.J.; Kimball, R.W. OpenProp: An open-source design tool for propellers and turbines. In Proceedings of the 12th Propeller and Shafting Symposium, Williamsburg, VA, USA, 15–16 September 2009.
39. *ISO 15016:2015*; Ships and Marine Technology—Guidelines for the Assessment of Speed and Power Performance by Analysis of Speed Trial Data. ISO: Geneva, Switzerland, 2015.
40. Stannat, W. On the Convergence of Genetic Algorithms—A Variational Approach. *Probab. Theory Relat. Fields* **2004**, *129*, 113–132. [CrossRef]